Finite Element Thermal Design of the Hexafly-INT Experimental Flight Test Vehicle

Valerio Carandente, Roberto Scigliano*, Giuseppe Pezzella*, Marco Marini* and Johan Steelant***
**Italian Aerospace Research Centre (CIRA)*
Via Maiorise snc, 81043 Capua, Italy
*** European Space Agency (ESA)*
Keplerlaan 1, 2201 AZ Noordwijk, Netherlands

Abstract

The Hexafly-INT project intends to test in free-flight conditions an innovative gliding vehicle with several breakthrough technologies on-board. This approach will create the basis to gradually increase the readiness level of a consistent number of technologies suitable for high-speed flying systems.
The paper presents a Finite Element thermal analysis of the Experimental Flight Test Vehicle, combining information coming from the flight trajectory, the vehicle aerothermodynamics and the materials behaviour in high temperature conditions. Numerical results show the thermal performances of the selected high temperature resistant materials in the moderate enthalpy flow conditions and provide fundamental information on the thermal loads to be considered for structural analyses.

1. Introduction

Over the last years, innovative concepts of civil high-speed transportation vehicles and the development of related technologies were proposed in EC co-funded projects like ATLLAS, LAPCAT and HEXAFLY [1,2,3]. These vehicles have a strong potential to increase the cruise range efficiency at high Mach numbers, thanks to efficient propulsion units combined with high-lifting vehicle concepts [4,5].
Nonetheless, performing a flight test will be the only and ultimate proof to demonstrate the technical feasibility of these new promising concepts and technologies and would result into a major breakthrough in high-speed flight. At present, the expected performances are usually demonstrated by numerical simulations and only partly by experimental tests. As high-speed wind tunnels are intrinsically limited in size, it is nearly impossible to completely fit even modest vehicle planform into a tunnel. Though numerical simulations are less restrictive in geometrical size, they struggle however with accumulated uncertainties in their modelling, making predictions doubtful without in-flight validation. As a consequence, the obtained technology developments are now limited to a Technology Readiness Level (TRL) equal to 4 (components validated in laboratory).
The HEXAFLY-INT project aims at the free flight testing of an innovative high-speed vehicle with several breakthrough technologies on board [6,7]. This approach will create the basis to gradually increase the TRL.
The vehicle design, manufacturing, assembly and verification will be the main driver and challenge in this project, in combination with a mission tuned sounding rocket. The prime objectives of this free-flying high-speed cruise vehicle shall aim at [4]:

- a conceptual design demonstrating a high aerodynamic efficiency at cruise conditions with a high volumetric efficiency;
- a positive aerodynamic balance at a controlled cruise Mach numbers from 7 to 8;
- a good gliding performance from Mach 7 to 2;
- an optimal use of advanced high-temperature resistant materials and/or structures.

The main flight sequence profile and mission events are shown in Figure 1 and listed in Table 1 [5,8,9]. In particular, from Figure 1 and Table 1 it is evident that the separation between the launcher and the whole vehicle, consisting of the Experimental Flight Test Vehicle (EFTV) and the Experimental Support Module (ESM), occurs around the apogee of the sounding rocket parabolic trajectory. Then, in the first part of the descent, the vehicle attitude is controlled by the Cold Gas System (CGS) included in the ESM. When the dynamic pressure along the flight path is large enough to guarantee the aerodynamic manoeuvrability of the EFTV, the ESM is released. Finally, after a pull-out manoeuvre, the EFTV starts its aerodynamically controlled cruise flight. The analysed EFTV and ESM configurations are depicted in Figure 2 [8].

In the present work the methodology and the implementation of tools for the thermal analysis of the EFTV, during the considered flight path, is presented [9]. Thermal analyses are performed on the basis of the trajectory provided by Gas Dynamics Limited (GDL), reported in Section 2, and of the CFD aerothermodynamic calculations presented in Section 3. The preliminarily selected high temperature resistant materials are described in Section 4, while in Section 5 the numerical procedure for the thermal analysis is described and its results reported. The calculations show a first feasibility analysis for the preliminarily selected materials.

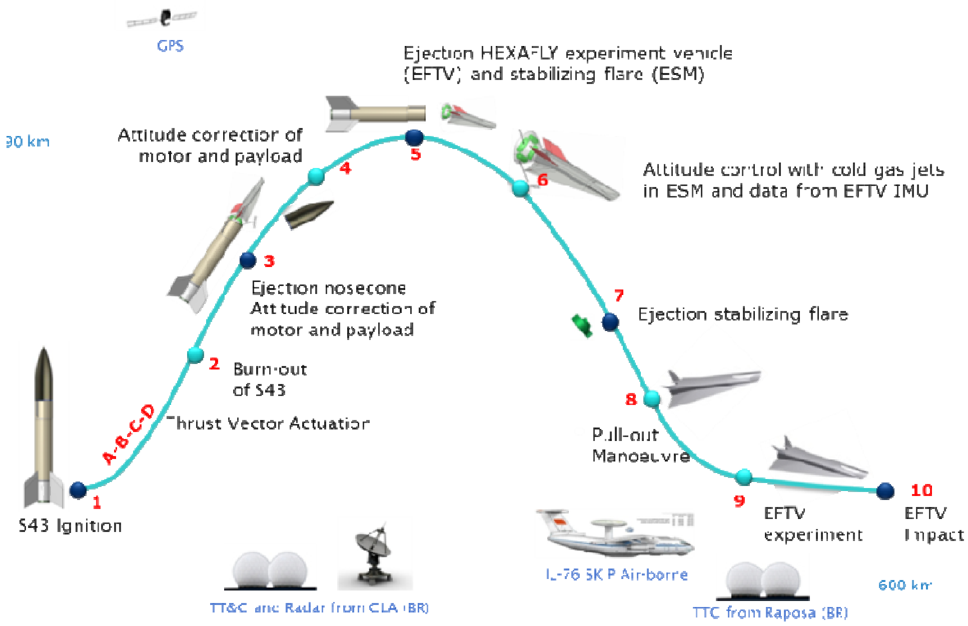

Figure 1: Flight sequence profile [5]

Table 1: Flight sequence events [5]

#	Flight Event
1-2	Propelled ascent
2	S43 motor burnout
3	Nose-cone ejection
4	L/V alignment
5	ESM/EFTV release
6	Attitude control by CGS in the ESM
7	Ejection of ESM
8	Pull-out manoeuvre
9	Controlled flight
10	Impact

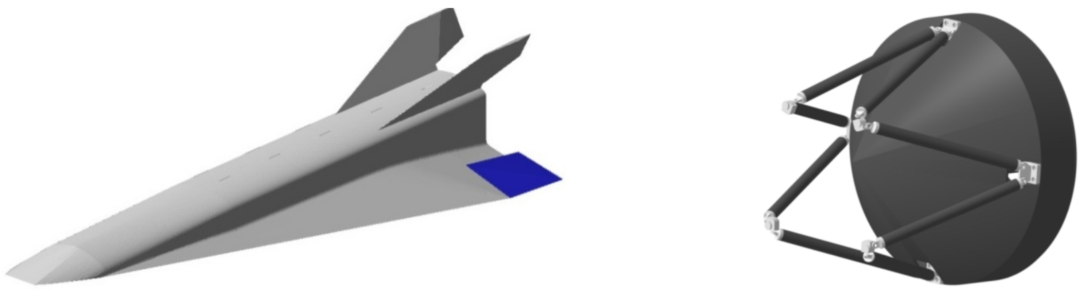

(a) (b)

Figure 2: EFTV (a) and ESM (b) configurations

2. Flight Trajectories

Flight mechanic analyses developed so far refer to different altitudes of the ESM release from the EFTV. For instance, Figure 3 shows the trajectory obtained for an EFTV mass of 350 kg assuming the ESM ejection at 50 km altitude. In particular, Figure 3 provides the time histories of altitude and velocity during descent, starting from the ESM release. This preliminary trajectory results in the most conservative scenario in terms of aero-thermal and mechanical loads available so far. Indeed, the profile of the EFTV stagnation point convective heat transfer coefficient, provided as input to the thermal analysis hereinafter discussed in non-dimensional form, is shown in Figure 4. It was derived from the corresponding convective heat flux, estimated by means of the Tauber's [10] relationship throughout the descent flight shown in Figure 3. The EFTV nose leading edge radius is $2 \cdot 10^{-3}$ m and the aerothermal loading conditions refer to radiative cooled walls with a surface emissivity of 0.4.

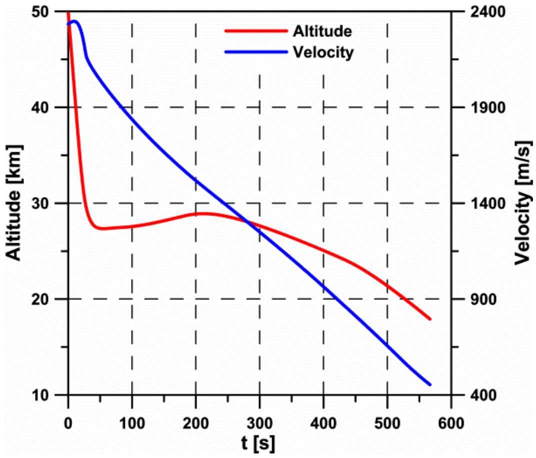

Figure 3: Altitude and velocity profiles for the considered flight path of the EFTV vehicle

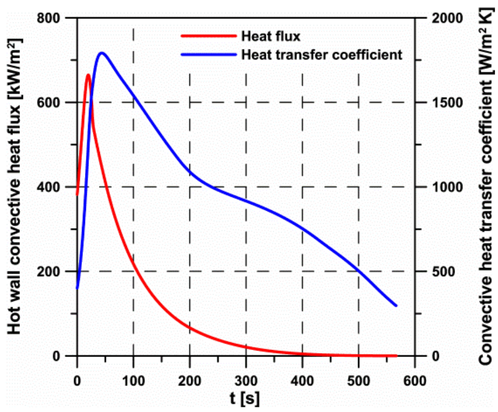

Figure 4: Stagnation point convective heat flux estimated by means of Tauber's formula (radiation equilibrium condition) and the corresponding convective heat transfer coefficient along the considered flight path

A preliminary assessment of laminar-to-turbulent transition has been also performed. Boundary layer transition is usually based on local flow conditions such as local Mach and Reynolds numbers. However, because the assessment of the local flow condition demands very accurate CFD computations which are out of the present design effort, a transition method [11], based on free-stream Reynolds (Re_∞) and Mach numbers (M_∞) and reported in Equation (1), has been adopted. In Equation (1) Re_T and C_m depend on the type of flow, angle of attack, leading edge sweep angle, and leading edge nose bluntness.

$$\log Re_\infty > [\log Re_T + C_m(M_\infty)] \quad \textbf{(1)}$$

According to this transition criterion, turbulent flow conditions are expected for the EFTV glider below about 30 km altitude.

3. Aerothermodynamic Calculations

CFD calculations have been therefore carried out in fully turbulent flow conditions, assuming the radiation equilibrium temperature at the vehicle walls with a surface emissivity of 0.4, in the trajectory flights conditions listed in Table 2. Note that time is counted from ESM/EFTV separation at 50 km altitude. As results, surface distributions of the convective heat transfer coefficient have been implemented as inputs for the subsequent thermal analyses.

Table 2: Asymptotic condition for CFD aerothermodynamic calculations

Flight Condition	Time (s)	Altitude (km)	Mach number (-)	Angle of Attack (°)
Max Angle of Attack	27.0	29.9	7.25	12.0
Max Aerodynamic efficiency	32.0	28.7	7.10	3.62
Max Stagnation point heat flux	36.0	28.0	7.03	1.63

Numerical analysis of the flowfield past the EFTV was performed on hybrid meshes, composed by tetrahedra in the flow and prisms in the boundary layer near the walls. The overall number of cells is about 10 million for half configuration. The distribution of surface grid points was dictated by the level of resolution desired in various areas of vehicle such as the stagnation region, the nose and the tail leading edges, according to the computational goals and requirements. Grid refinement in regions of flowfield characterized by strong gradients was made through a solution adaptive approach. Indeed, an iterative shock-fitting procedure is carried out in order to properly accommodate the bow shock shape. The air is modelled as an ideal gas. Indeed, the ideal gas assumption can be considered still valid in this case, considering that the Mach number here considered is less than 8. In addition, the EFTV aeroshape features a very slender configuration (leading edge radius of 2 mm) that shall fly at rather low angle of attack (i.e. behind a weak attached bow shock). The surface distributions of pressure and convective heat transfer coefficient obtained in the maximum angle of attack condition are reported in Figure 5 and Figure 6, respectively, as exemplary of the whole set of CFD aerothermodynamic results obtained.
Surface pressure and convective heat transfer coefficient contours point out that the vehicle nose, the wing leading edge and the aileron are the most solicited vehicle parts, while on the remaining aeroshape a quite smooth evolution of loading conditions is expected.

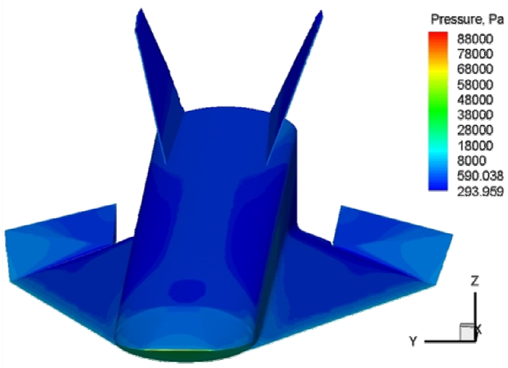

Figure 5: Pressure contour (Pa) in the maximum angle of attack condition

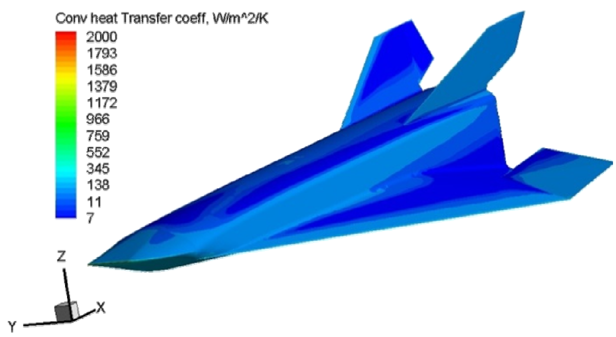

Figure 6: Convective heat transfer coefficient (W/m^{2}K) in the maximum angle of attack condition

4. EFTV Candidate Materials

Different classes of materials have been preliminarily selected and analysed for the EFTV structure, namely: titanium alloy, copper, C/C-SiC and zirconia for surface coatings.
Titanium alloys exhibit a unique combination of mechanical and physical properties and corrosion resistance which have made them desirable for critical, demanding aerospace applications, also in high temperatures conditions. A high temperature resistant copper is employed as a heat sink to accommodate the thermal energy in some critical components (e.g. nose and leading edges). C/C-SiC developed at DLR and tested in different high temperatures applications (e.g. HIFiRE and SHEFEX) is considered for ailerons and for the largest part of the wing leading edge [12]. A zirconia coating layer has been also considered to protect titanium and copper components, increasing the surface emissivity and confining the larger temperatures on the layer itself.

Thermal and mechanical properties of titanium alloy and zirconia coating have been provided by TsAGI, Tsentralniy Aerogidrodinamicheskiy Institut (Central Aerohydrodynamic Institute), which is in charge of the system manufacturing.
In particular, the following assumptions, summarized in Table 3, have been carried out on the vehicle components shown in Figure 7:

- copper for the vehicle nose;
- copper for the fore part of the wing leading edges;
- C/C-SiC for the remaining part of the wing leading edge;
- copper for the leading edge of the tails;
- C/C-SiC for the ailerons;
- titanium alloy for the remaining part of the structure.

In addition, as previously mentioned, a layer of 1 mm thick zirconia has been foreseen for all the components in titanium alloy and copper. Using a conservative approach, a constant surface emissivity of 0.4 has been set for the external coated surfaces.

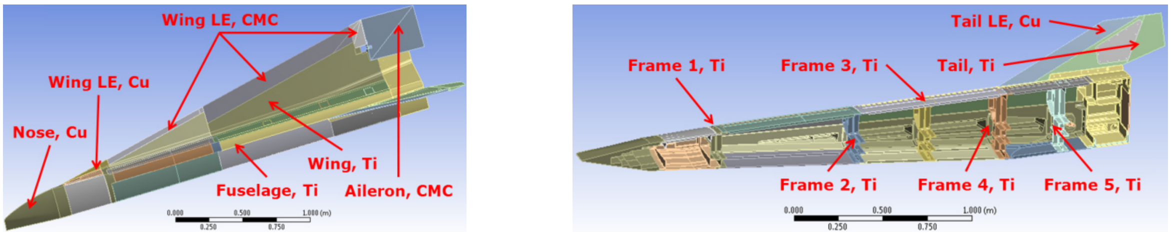

Figure 7: Main structural components of the analysed EFTV

Table 3: Preliminarily material assignment for the main structural components

Nose	Fuselage	Wing	Wing LE	V-Tail	Aileron
Copper	Ti-Alloy	Ti-Alloy	C/C-SiC / Copper	Ti-Alloy / Copper	C/C-SiC

5. Thermal Analysis

5.1 Numerical Procedure

The vehicle thermal behaviour has been preliminary assessed by means of the Finite Element Method (FEM) implemented in the software Ansys [13,14]. A transient analysis along the computed entry path is performed to evaluate the time dependent temperature of the structure. In synthesis, as also schematically reported in Figure 8, the following procedure has been carried out:

- the available CAD drawing of the vehicle is implemented in Ansys Workbench and properly modified, if required;
- the computational mesh for the subsequent analyses is generated;
- the transient thermal analysis is set assuming as boundary condition the convective heat transfer coefficient spatial distribution over the vehicle surface, evaluated in a certain number of flight conditions by means of stationary CFD calculations. These distributions are properly scaled by the stagnation-point heat transfer coefficient variation along the trajectory, normalized with respect to the corresponding reference condition (see Figure 8). A radiative dissipation condition is also considered for all the external surfaces;
- static structural computations can be then carried out, if required, in the most critical conditions along the trajectory, assigning as boundary conditions the temperature distributions previously evaluated at selected instants along the trajectory and the pressure distribution resulting from CFD analyses.

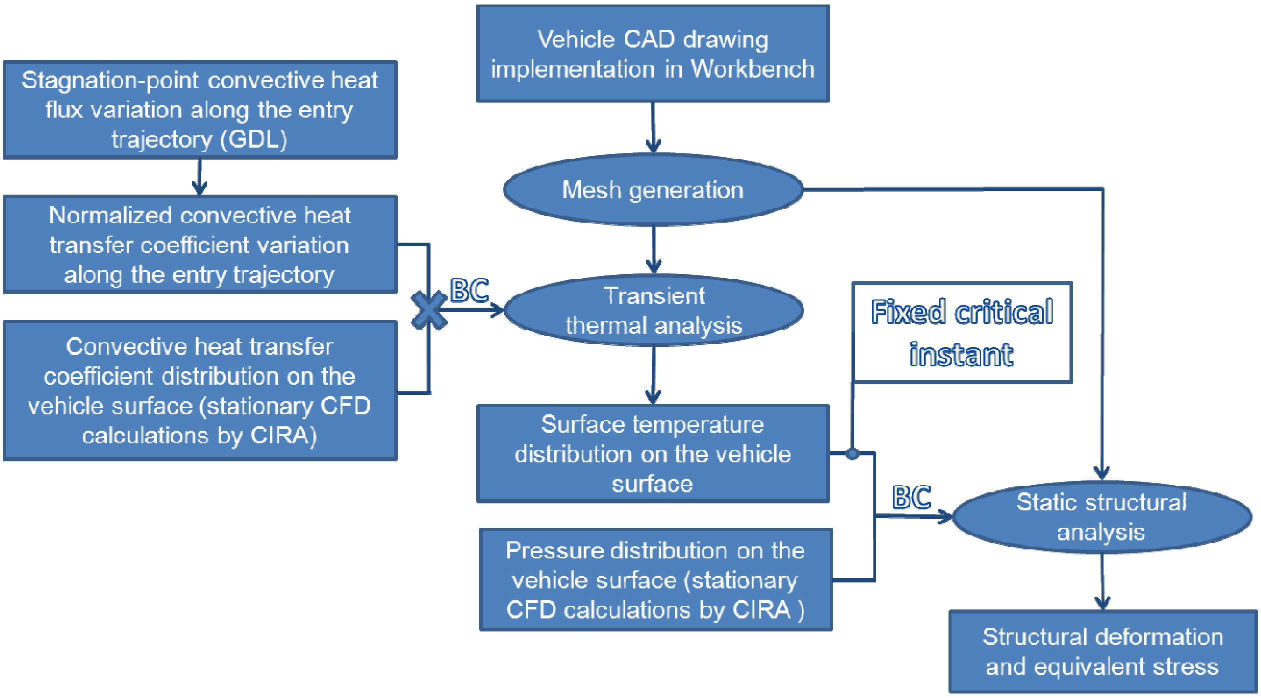

Figure 8: Numerical procedure flow chart

It is now worth underlining that, as previously mentioned, the heat flux boundary conditions for the transient thermal analysis has been assigned in terms of the convective heat transfer coefficient, so that the numerical code can take into account the effective heat flux entering the structure as the wall temperature increases under the heating process (see Equation 2). Equation 2 also assumes an ideal gas with constant specific heat.

$$\dot{q} = h \cdot (T_0 - T_w) \approx \frac{\dot{q}_{cw}}{T_0} \cdot (T_0 - T_w) = \frac{\dot{q}_{hw,eq}}{T_0 - T_{w,eq}} \cdot (T_0 - T_w) \qquad \textbf{(2)}$$

It is clear that the convective heat transfer coefficient at any point of the vehicle surface and at a certain time instant is assigned multiplying the value at that spatial point (resulting from the CFD calculation) by the normalized stagnation-point convective heat transfer coefficient along the flight path at the selected time instant.

5.2 Preliminary Results

As results, according to the previously discussed method, the temporal variation of the maximum temperature on the different analysed materials and vehicle components has been plotted along the flight path. Figure 9 reports in particular the maximum temperature variation along the flight profile on the main vehicle components.
From Figure 9 it can be seen that zirconia coatings and C/C-SiC components (having maximum service temperatures in the order of 2400°C and 1600°C, respectively) would widely survive the aerothermal environment in these conditions. On the other hand, it can be noted that the maximum temperatures on the titanium and copper structures slightly exceed their upper working temperature limits (600 and 800°C, respectively), but only in limited spots of the vehicle, coloured in red for the titanium structure in Figure 10. This means that such temperature overshoot can be in principle redistributed inside the vehicle structure through a future thermal structural optimization.

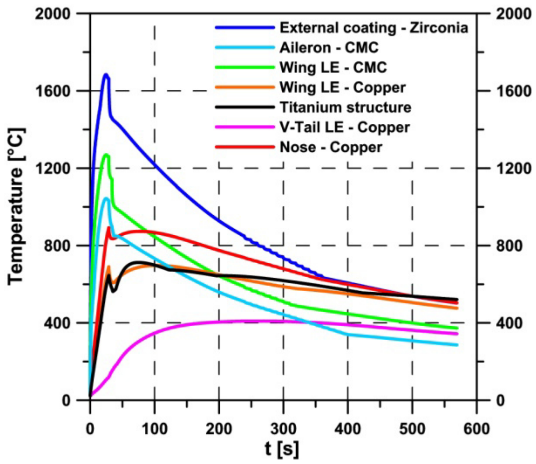

Figure 9: Maximum temperature along the flight profile on the main vehicle components

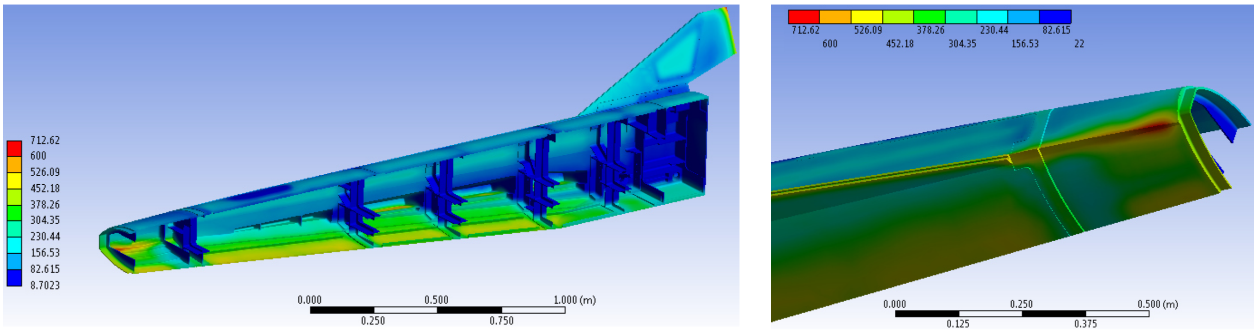

Figure 10: Temperature distribution on the titanium structure at the peak heating condition for titanium components

6. Conclusions

Finally, it can be concluded that:

- a thermal model has been realized for the entire structure on the basis of aerothermal loads estimated along the flight path;
- zirconia coating guarantees a relatively large surface emissivity and a suitable thermal protection for the underlying materials;
- copper seems to be adequate for the nose and the first part of the wing leading edge, considering its ability to work as a heat sink;
- copper and titanium structures can withstand the aerothermal environment except for limited spots, requiring a proper thermal structural optimization;
- thermal structural design is still ongoing and a numerical analysis campaign will be perform on updated structural configuration.

7. Acknowledgments

This work was performed within the 'High-Speed Experimental Fly Vehicles-International' project fostering International Cooperation on Civil High-Speed Air Transport Research. HEXAFLY-INT, coordinated by ESA-ESTEC, is supported by the EU within the 7th Framework Programme Theme 7 Transport, Contract no.: ACP0-GA-2014-620327 and by the Ministry of Industry and Trade, Russian Federation. Further info on HEXAFLY-INT can be found on http://www.esa.int/hexafly-int.

References

[1] Steelant J. 2009. Achievements obtained on Aero-Thermal Loaded Materials for High-Speed Atmospheric Vehicles within ATLLAS. In *16th AIAA/DLR/DGLR International Space Planes and Hypersonic Systems and Technologies Conference*.

[2] Steelant, J. 2011. Sustained Hypersonic Flight in Europe: first achievements within LAPCAT II. In *17th AIAA "International Space Planes and Hypersonic Systems and technologies conference*.

[3] Steelant, J. et al. 2015. Conceptual Design of the High-Speed Propelled Experimental Flight Test Vehicle HEXAFLY. In *20th AIAA International Space Planes and Hypersonic Systems and technologies conference*.

[4] Hexafly-INT Team. 2014. Part B "High-Speed Experimental Fly Vehicles–INTernational". CIRA-CF-14-1132.

[5] Jung, W., Ettl, J., Kallenbach, A., Turner, J. 2014. Mission Definition and System Requirements, WP 2.0 – Launch Vehicle. In *HEXAFLY-INT MDR & SRR*.

[6] Favaloro, N., Pezzella, G., Carandente, V., Scigliano, R., Cicala, M., Morani, G., Steelant, J. 2015. Design Analysis of the High-Speed Experimental Flight Test Vehicle HEXAFLY-International. In *20th AIAA International Space Planes and Hypersonic Systems and Technologies Conference*.

[7] Pezzella, G., Marini, M., Reimann, B., Steelant, J. 2015. Aerodynamic Design Analysis of the HEXAFLY-INT Hypersonic Glider. In *20th AIAA International Space Planes and Hypersonic Systems and Technologies Conference*.

[8] Pezzella, G., van Brummen, S., Steelant, J. 2015. Assessment of Hypersonic Aerodynamic Performance of the EFTV-ESM Configuration in the Framework of the Hexafly-Int Research Project. In *8th European Symposium on Aerothermodynamics for Space Vehicles*.

[9] Pezzella, G., Carandente, V., Scigliano, R., Marini, M., Steelant, J. 2015. Aerothermal Environment Methodology of the Hexafly-Int Experimental Flight Test Vehicle (EFTV). In *8th European Symposium on Aerothermodynamics for Space Vehicles*.

[10] Tauber, M.E. 1989. A review of high-speed, convective, heat-transfer computation methods. NASA Technical Paper 2914.

[11] Quinn, R.D., Gong, L. 1990. Real-Time Aerodynamic Heating and Surface Temperature Calculations for Hypersonic Flight Simulation. NASA Technical Memorandum 42522.

[12] Glass, D.E., Capriotti, D.P., Reimer, T., Kütemeyer, M., Smart, M. 2014. Testing of DLR C/C-SiC and C/C for HIFiRE 8 Scramjet Combustor. In 19th AIAA International Space Planes and Hypersonic Systems and Technologies Conference.

[13] ANSYS Inc. 2009. Thermal analysis guide, Release 12.1.

[14] ANSYS Inc. 2009. Structural analysis guide, Release 12.1.